THE JOURNAL OF PHYSICAL CHEMISTRY B

Article

pubs.acs.org/JPCB

Redox-Induced Conformational Switching in Photosystem-II-Inspired Biomimetic Peptides: A UV Resonance Raman Study

Cynthia V. Pagba and Bridgette A. Barry*

School of Chemistry and Biochemistry and the Parker H. Petit Institute of Bioengineering and Biosciences, Georgia Institute of Technology, Atlanta, Georgia 30332, United States

Supporting Information

ABSTRACT: Long-distance electron transfer (ET) plays a critical role in solar energy conversion, DNA synthesis, and mitochondrial respiration. Tyrosine (Y) side chains can function as intermediates in these reactions. The oxidized form of tyrosine deprotonates to form a neutral tyrosyl radical, $Y^{\bullet}$, a powerful oxidant. In photosystem II (PSII) and ribonucleotide reductase, redox-active tyrosines are involved in the proton-coupled electron transfer (PCET) reactions, which are key in catalysis. In these proteins, redox-linked structural dynamics may play a role in controlling the radical's extraordinary oxidizing power. To define these dynamics in a structurally tractable system, we have constructed biomimetic peptide maquettes, which are inspired by PSII. UV resonance Raman studies were conducted of ET and PCET reactions in these β-hairpins, which contain a single tyrosine residue. At pH 11, UV photolysis induces ET from the deprotonated phenolate side chain to solvent. At pH 8.5, interstrand proton transfer to a π-stacked histidine accompanies the Y oxidation reaction. The UV resonance Raman difference spectrum, associated with Y oxidation, was obtained from the peptide maquettes in D_2O buffers. The difference spectra exhibited bands at 1441 and 1472 cm^{-1}, which are assigned to the amide II′ (CN) vibration of the β-hairpin. This amide II′ spectral change was attributed to substantial alterations in amide hydrogen bonding, which are coupled with the $Y/Y^{\bullet}$ redox reaction and are reversible. These experiments show that ET and PCET reactions can create new minima in the protein conformational landscape. This work suggests that charge-coupled conformational changes can occur in complex proteins that contain redox-active tyrosines. These redox-linked dynamics could play an important role in control of PCET in biological oxygen evolution, respiration, and DNA synthesis.

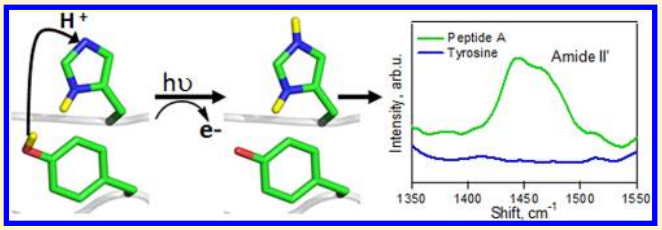

INTRODUCTION

Redox-active tyrosine (Y) residues facilitate long-distance electron transfer (ET) reactions in biological systems such as photosystem II (PSII),[1−3] ribonucleotide reductase (RNR),[4] and prostaglandin synthase.[5,6] At pH values greater than 10, the phenolic side chain is deprotonated, and the tyrosinate side chain is oxidized by an ET reaction, which forms a neutral tyrosyl radical, $Y^{\bullet}$. Proton-coupled electron transfer (PCET) occurs when oxidation of tyrosine occurs at physiological pH values. Under these conditions, the ET reaction is coupled with the deprotonation of the phenolic oxygen (Figure 1A), again generating a neutral radical.[7,8] $Y^{\bullet}$ can serve as a strong oxidant[9] and can be used to drive difficult biological reactions, such as photosynthetic water oxidation or ribonucleotide reduction. In PCET, the identity of the proton acceptor modulates the energetics and kinetics of the reaction (Figure 1A). For example, differences in the surrounding protein matrix and water accessibility give rise to alterations in the midpoint potential, when the catalytically relevant redox-active tyrosines are compared (reviewed in ref 3).

Oxidation of the aromatic ring alters the electronic charge distribution of the phenolic ring,[10] and oxidation may be coupled with significant changes in the backbone and ring dihedral angle.[11] This charge density difference and accompanying rotational motion may significantly alter the immediate environment of Y. For example, EPR,[12] FT-IR,[13] and UV resonance Raman (UVRR)[11] studies of the redox-active tyrosine in ribonucleotide reductase predict a change in Y conformation when Y is oxidized and reduced. This rotation provides a way to regulate PCET through changes in interacting hydrogen bonds.[11] In PSII, there are two redox-active tyrosine residues, YZ, the oxidant of the Mn_4CaO_5 oxygen-evolving center (OEC), and YD. It has been proposed that conformational changes accompany the YZ redox reaction and provide a control mechanism by which the OEC controls the YZ midpoint potential.[3]

It is difficult to obtain high-resolution structural information about the reactive, radical-containing states of complex proteins. Biomimetic peptides, known as maquettes, provide a structurally tractable framework in which to investigate these questions. Previous studies of redox-active amino acid residues, such as tyrosine and tryptophan, in peptide maquettes have focused on α-helical peptides.[14−16] β-hairpin peptides provide

Special Issue: Richard A. Mathies Festschrift

Received: April 14, 2012
Revised: July 6, 2012

   dx.doi.org/10.1021/jp303607b | J. Phys. Chem. B XXXX, XXX, XXX−XXX

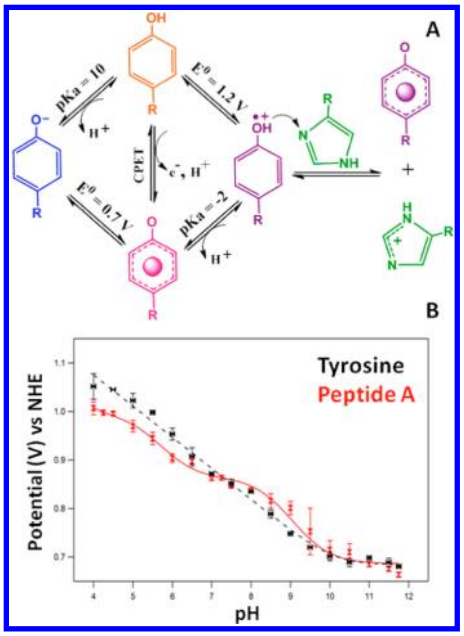

Figure 1. (A) Thermodynamic diagram illustrating PCET and ET reactions in tyrosine (red, top) and the tyrosinate (blue, left) side chain, respectively. The potentials (versus NHE) were reported for tyrosinate at pH 10 and for tyrosine at pH 2.[8] Oxidation of tyrosine at pH values below the phenolic pKa leads to coupled electron and proton transfer (CPET, middle) if the electron and proton are transferred in one kinetic step. The proton acceptor is shown as the imidazole side chain of histidine (right), relevant to PCET in the β-hairpin maquettes. (B) Effect of pH on the peak potential of the anodic waves, as assessed by square-wave voltammetry, of peptide A (red) (reproduced from ref 10). The inflection points (attributed to histidine pKa values) are attributed to a mid-pH-range PCET reaction between tyrosine and the imidazole ring.[10] The pH dependence of peak potentials for tyrosine (black) is also presented for reference (reproduced from ref 10).

another important approach with which to investigate effects on solution structure and dynamics.[17] In our previous work, we constructed an 18 amino acid, β-hairpin maquette, which contains a single tyrosine and histidine. This maquette carries out a PCET reaction, which leads to histidine protonation, when tyrosine is oxidized in the mid-pH range.[10,18] This was concluded from square-wave voltammetry, which showed unique inflection points, not observed for tyrosine, in the pH titration (Figure 1B).

UVRR is an incisive technique in determining the structure and function of peptides and proteins.[19] Raman spectroscopy is advantageous in the study of aqueous samples because the Raman signal of water is weak. Potentially troublesome background fluorescence, commonly encountered using visible excitation of proteins, is eliminated using UV probe wavelengths.[20−22]

In this article, UVRR is used to study β-hairpin maquettes, in which ET and PCET reactions occur. Using difference techniques, we find that oxidation of Y is accompanied by amide hydrogen-bonding changes, consistent with a secondary structural change in the β-hairpin. These experiments suggest that a redox-coupled conformational switch occurs in tyrosine-containing peptides and proteins.

MATERIALS AND METHODS

Materials. The 18-mer peptides were synthesized by solid-state synthesis and were obtained from Genscript USA Inc. (Piscataway, NJ) and New England Peptide (Gardner, MA). The dipeptides were obtained from Bachem Inc. (Torrance, CA). Samples were suspended in a H_2O/D_2O buffer containing 5 mM sodium borate or *N*-cyclohexyl-3-aminopropanesulfonic acid (CAPS), pH/pD 11, or 5 mM *N*-tris(hydroxymethyl)-methyl-3-aminopropanesulfonic acid (TAPS), pH/pD 8.5, to give 1 mM solutions. The pD is reported as the uncorrected meter reading because the small solvent isotope effects on weak acid pKa values are compensated for by the D_2O-induced change in response of the glass pH electrode.[23−25]

UVRR Measurements. The spectra were obtained at room temperature using a 244 nm probe beam. The probe beam (244 nm) was generated from an intracavity frequency-doubled argon ion laser (Cambridge LEXEL 95, Fremont, CA). The probe was coupled to a Raman microscope system (Renishaw inVia, Hoffman Estates, IL) equipped with UV-coated, deep depletion charge-coupled device. Backscattering from the sample was collected by a 15× UV (N.A. 0.32) objective (OFR division of Thorlabs, Inc., Caldwell, NJ), assembled in a Leica Microsystems (Buffalo Grove, IL) microscope. The spectral resolution was 6 cm^{-1}, and the separation between the data points was 3.8 cm^{-1}. To prevent sample damage due to UV irradiation, the peptide samples were recirculated using a peristaltic pump through a nozzle (~120 μm inner diameter) to form a jet. The volume of the circulating solution was 1 mL. The flow rate was 4.5 mL/min, and the pump was plumbed with silicone tubing. For more details, see refs 20 and 21.

The radical was photogenerated by increasing the power of the UV probe beam, as described previously.[26] The high power-minus-low power difference spectrum was obtained by subtracting an averaged low-power scan (340 μW) from an averaged high-power scan (3.4 mW). A total of 16 low-power scans (240 s) and 8 high-power scans (120 s) were averaged, respectively, from an 8 mL sample. For each 1 mL sample aliquot, a low-power scan was obtained first, followed by high-power scan and then another low-power scan. The amplitude of the averaged low-intensity scan was multiplied by a factor of 5 before subtraction to give the difference spectrum (radical-minus-singlet). This multiplication factor accounts for the difference in probe intensity and the number of scans and corresponds to the intensity changes in the solvent D_2O band, which was used as an internal standard. Sulfate could not be used as a Raman standard with the β-hairpins due to a change in their solubility under those conditions. The measurements were performed twice or thrice on different samples, and the difference spectra obtained were averaged to give the final signal-to-noise.

See Supporting Information Figure S1 for examples of the high- and low-power spectra, acquired from tyrosinate, and Figure S2 (Supporting Information) for examples of difference spectra, acquired from tyrosinate in H_2O and D_2O.

RESULTS

Figure 2A shows the primary sequence of peptide A (IMDRYRVRNGDRIHIRLR). This peptide contains a single tyrosine residue (Y5) (Figure 2A), which is hydrogen-bonded to arginine 16, and exhibits $\pi-\pi$ and $\pi-$cation interactions with histidine 14 and arginine 12, respectively (Figure 2E and F). The NMR structure of peptide A confirms a β-hairpin fold

dx.doi.org/10.1021/jp303607b | J. Phys. Chem. B XXXX, XXX, XXX−XXX

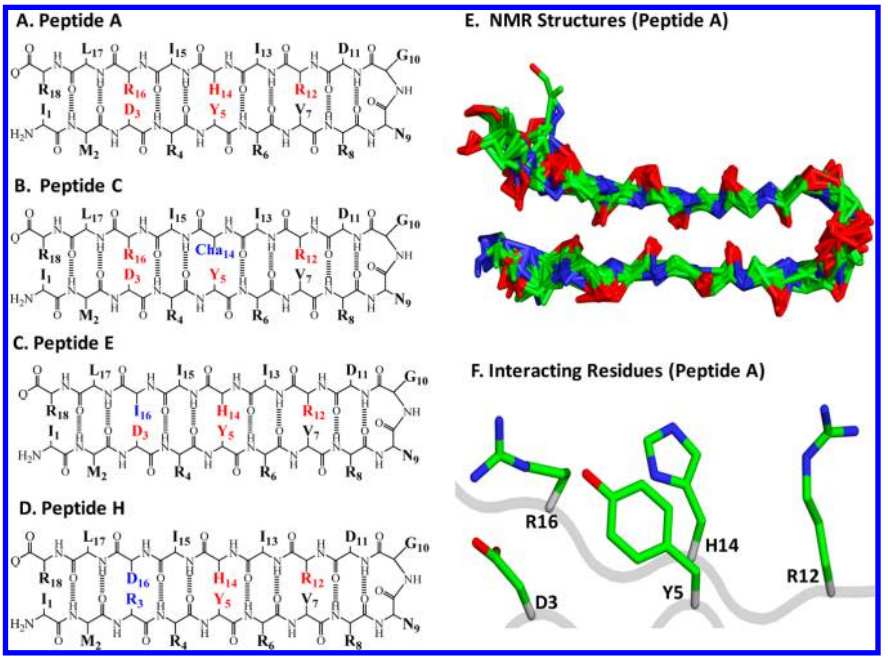

Figure 2. (A) Primary sequence of peptide A, IMDRYRVRNGDRIHIRLR. The residues involved in the cross-strand interaction are in red. (B–D) Amino acid substitutions (in blue), which alter cross-strand interactions in peptides C (B), E (C), and H (D). In peptide C, His14 was replaced with cyclohexylalanine (Cha). (E) Lowest-energy NMR structures of peptide A.[10] (F) Intermolecular interactions in the lowest-energy structure of peptide A showing the cross-strand interactions between Y5 and H14 ($\pi-\pi$), Y5 and R12 (π–cation), Y5 and R16 (H-bond), and the salt-bridge formed by D3 and R16.

(Figure 2E and F). Variants of this peptide were generated by solid-state synthesis, and their primary sequences are compared in Figure 2B–D. In peptide C (Figure 2B), histidine was replaced with cyclohexylalanine (Cha). In peptide E (Figure 2C), a hydrogen-bonding interaction between arginine 16 and tyrosine was removed, as well as the salt bridge between arginine 16 and aspartate 3. In peptide H (Figure 2F), the salt bridge between aspartate 3 and arginine 16 was reversed. Our previous CD and thermal melting experiments on peptides A, C, and E indicated that these peptides fold to give a β-hairpin both at pH 5 and 11.[18] CD studies and thermal melts of peptide H at pH 5 and 11 gave a similar result (data not shown).

Figure 3 presents the UVRR spectra of tyrosine and β-hairpin peptides as a function of pH and pD. With 244 nm Raman excitation, the Raman probe is on resonance with the La transition of the tyrosine ring (~240 nm at pH $\geq$ 10 and 222 nm at pH $\leq$ 10)[27] and the weak n–π^* (210–230 nm)[28,29] transition of the peptide backbone. Other electronic transitions of the phenolic ring (~293 nm at pH > 10 and 275 nm at pH < 10)[27] and the peptide bond ($\pi-\pi^*$ at ~190 nm)[28,30] may be preresonantly enhanced at this excitation wavelength.

At pD 11, peptide A (Figure 3B, blue) exhibited characteristic vibrational bands of tyrosinate (Figure 3A, red), namely, 1174, 1207, and 1602 cm^{-1}, assigned to C–H bending (Y9a), tyrosine C_{ring}–CH_2– (Y7a), and ring stretching (Y8a), respectively (see ref 22 and references therein). At pH 8.5, peptide A (Figure 3D, purple) exhibited a new band at 1554 cm^{-1}, which was not observed in tyrosine (Figure 3C, green). This band shifted to 1441 and 1472 cm^{-1} in peptide A at pD 8.5 (Figure 3E, magenta). This ~100 cm^{-1} downshift in D_2O is characteristic of an amide II (H_2O, CN stretch/NH bend) and amide II′ (D_2O, CN stretch) assignment. Deuterium exchange uncouples the CN and NH bending modes and leads to a substantial downshift of the amide II band.[31] It can be observed

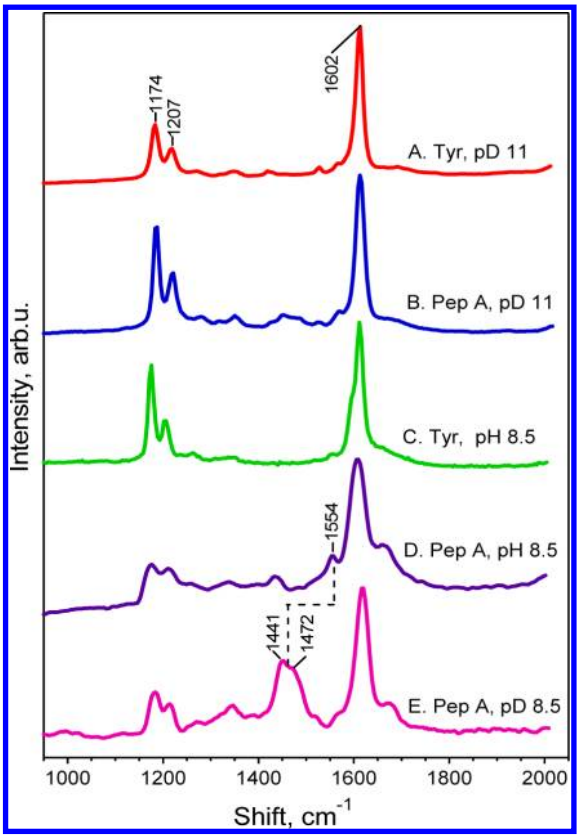

Figure 3. Representative UVRR spectra of (A) tyrosinate, pD 11, (B) peptide A, pD 11, (C) tyrosine, pH 8.5, (D) peptide A, pH 8.5, H_2O buffer, and (E) peptide A, pD 8.5, D_2O buffer. The 244 nm probe power was 3.4 mW.

dx.doi.org/10.1021/jp303607b | J. Phys. Chem. B XXXX, XXX, XXX–XXX

from the UVRR spectra in Figure 3D and E that the amide II′ band (predominantly C−N stretch) was more intense compared to the amide II (C−N stretch and N−H bending) mode when 244 nm excitation was employed. This intensity difference is consistent with expectations from previous UV Raman studies.[32−35]

The amide II′ has been observed previously with ∼240 nm Raman excitation in peptides and derivatives of acetamide.[32,35−37] Confirming these previous results, Figure 4

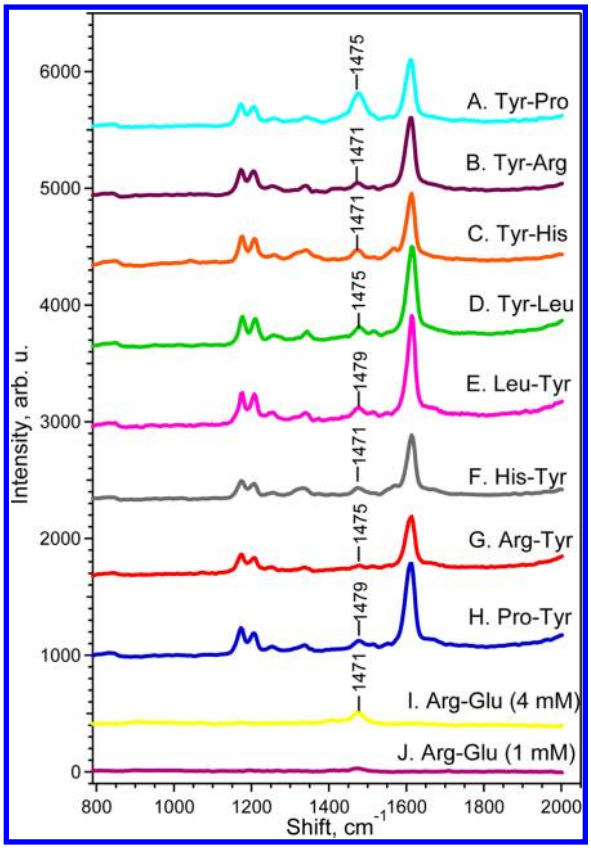

Figure 4. UVRR spectra of dipeptides at pD 8.5, D_2O buffer. The frequency of the amide II′ band is labeled in each spectrum. The 244 nm probe power was 3.4 mW. The spectra were acquired from two different samples and averaged.

shows that an amide II′ band, at 1471−1479 cm^{-1}, was observed in the 244 nm UVRR spectra of a series of tyrosine-containing dipeptides as well as the Arg-Glu dipeptide. Changes in frequency and intensity can be attributed in part to alterations in conformational distributions in the dipeptide. For example, the Tyr-Pro (A) and Pro-Tyr (H) exhibited clear differences in the amide II′ band intensity. This intensity change is attributed to the structural constraints imposed by the imide bond in the Tyr-Pro peptide. In addition, the absorbance of the X-Pro amide is red-shifted by ∼10 nm compared to other dipeptides. This red shift is expected to increase intensity through an increase in the Raman cross section.[38,39]

The pD dependence of the UVRR spectrum of the β-hairpins is explored in more detail in Figures 5 and 6. An increase in intensity of the tyrosinate bands was observed at pD 11, compared to that for tyrosine at pD 5 or 8.5. This enhancement is attributed to the red shift of the La transition of tyrosine, which has been described previously.[27,40] As expected, decreasing the pH downshifted the Y8a band of tyrosinate (1602 cm^{-1}) relative to tyrosine (1610 cm^{-1}) due to uncoupling of the ring and O−D vibrations.[41,42]

As shown in Figures 5 and 6, the intensity of the amide II′ feature was relatively constant as a function of pD. The band was observed both at high and low UV probe powers (Figure 6A and B). The additional peak at ∼1408 cm^{-1} in the pD 5 spectrum (Figure 6, red) is attributable to the N−D vibration of the deuterated histidine side chain.[43] This experiment shows that the spectral contributions due to the amide II′ band (∼1470 cm^{-1}) and to the deuterated histidine side chain (1408 cm^{-1}) can be distinguished. Excitation at 229 nm of peptide A at pD 11 (Supporting Information Figure S3) resulted in a more intense amide II′ band relative to the 244 nm probe, which is consistent with preresonance enhancement due to the $\pi-\pi^*$ amide transition.

UVRR difference spectroscopy was then used to study the effects of the Y redox reaction on the structure of the peptide. Only structural changes coupled to the redox reaction will be observed. Oxidation of tyrosinate was initiated by UV photolysis at pH 11. Figure S1 (Supporting Information) shows that the high-power scan exhibited the characteristic 1516 cm^{-1} CO band of the tyrosyl radical, which is generated by UV photolysis in the sample jet.[26] The ∼250 cm^{-1} upshift of the CO vibration is due to delocalization of unpaired spin onto the phenolic oxygen.[44] This spectrum was acquired in D_2O buffer.

Difference spectra, high power-minus-low power, were constructed to reflect the changes in frequency and/or amplitude associated with tyrosine oxidation. Such a tyrosine difference spectrum was obtained by subtracting the low-power scan (340 μW) from the high-power scan (3.4 mW) (Supporting Information Figure S2 and description of normalization in the Materials and Methods section). Positive bands were unique bands of the radical and were observed at 1408, 1516, and 1572 cm^{-1}, which correspond to C−H bending/C−C stretching, C−O$^{\bullet}$ stretching (Y7a), and C−C ring (Y8a) stretching modes, respectively.[13,26] Negative bands corresponded to the vibrational modes of the singlet tyrosine. It should be noted that difference spectra obtained from tyrosinate in H_2O and D_2O at pD 11 were very similar (Supporting Information Figure S2). Also, the spectra obtained from tyrosine and tyrosinate at pD 8.5 and pD 11, respectively, were similar (Figures 7A and 8A), except for the expected change of the Y8a frequency.

This approach was used to obtain the oxidation-induced difference spectra of tyrosine/tyrosinate in the Tyr-His dipeptide, peptide A, peptide C, peptide E, and peptide H at pD 8.5 (Figure 7) and 11 (Figure 8). At both pD values, tyrosine/tyrosinate (Figures 7A and 8A) and the Tyr-His dipeptide (Figures 7B and 8B) gave similar difference spectra that reflected the characteristic bands of the singlet and radical. These tyrosine and tyrosyl radical bands were also observed in the β-hairpins. In data acquired from peptide A (Figures 7C and 8C), additional negative bands at 1441 and 1472 cm^{-1} were observed in the difference spectra. The bands were observed in all of the peptides studied at pD 8.5, including peptide C (Figure 7). However, at pD 11, only the peptide A difference spectrum exhibited significant intensity in this region of the difference spectrum (Figure 8C). In peptide A at pD 11 (Figure 8C), the 1441 and 1472 cm^{-1} features were weaker than the bands observed in the pD 8.5 difference spectrum (Figure 7C). Note that because peptide C does not contain histidine, the 1440−1480 cm^{-1} spectral feature, observed in the

dx.doi.org/10.1021/jp303607b | J. Phys. Chem. B XXXX, XXX, XXX−XXX

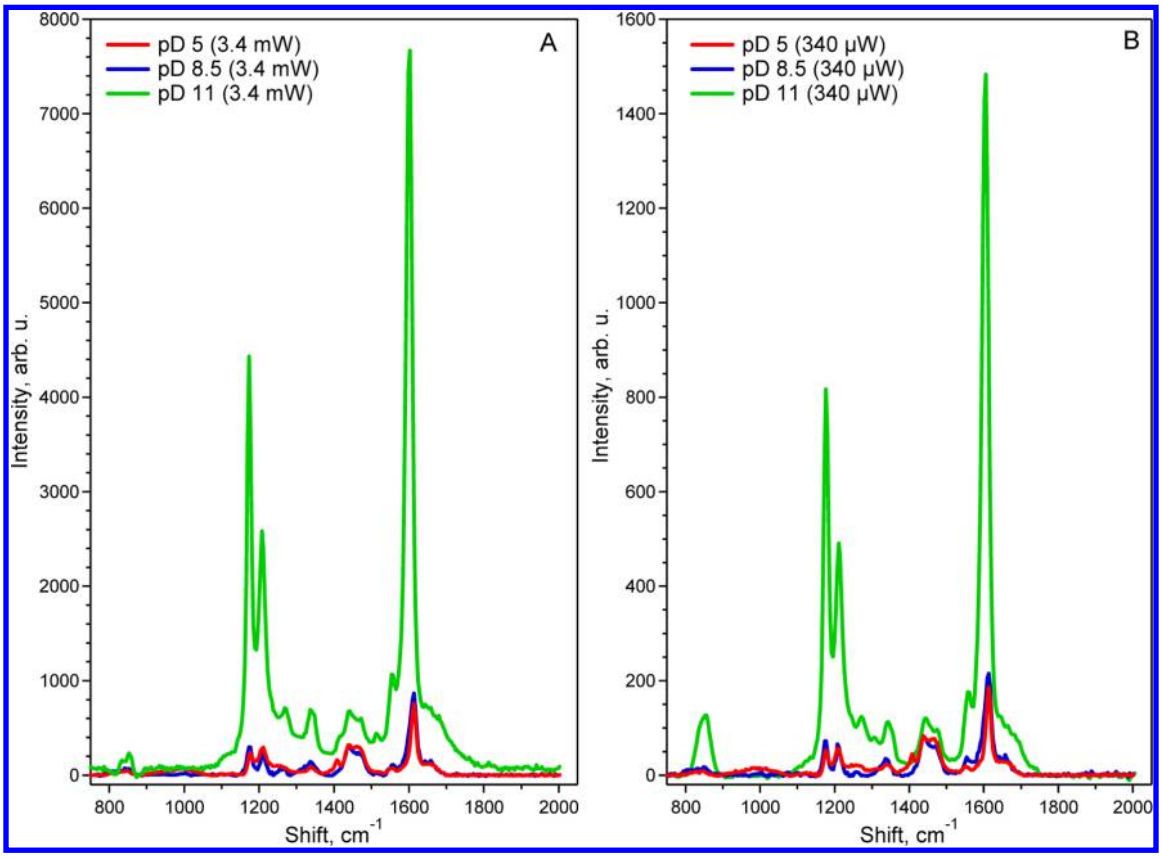

Figure 5. UVRR spectra acquired from peptide E (IMDRYRVRNGDRIHIILR), showing the pD dependence of the frequencies and intensity. The 244 nm probe power was 3.4 mW (A, left) or 340 μW (B, right). The pD 11 spectrum is in green, the pD 8.5 spectrum is in blue, and the pD 5.0 spectrum is in red.

pD 8.5 difference spectrum of this peptide (Figure 7D), does not arise from the histidine imidazole ring. The 1441 and 1472 cm^{-1} bands were not observed in peptides C, E, and H at pD 11 (Figure 8D–F).

The negative 1440–1480 cm^{-1} bands, observed in the difference spectra, are assigned to amide II′ bands, which contribute to the difference spectra due to an oxidation-induced change in secondary structure. Interestingly, difference spectra acquired from other peptide variants (C, E, and H, sequences Figure 2B–D) exhibited significant amide II′ bands only at pD 8.5.

To determine if the spectral changes observed were due to irreversible denaturation of the peptides, induced by the high-power UV probe beam, a control experiment was performed. Circular dichroism (CD) spectroscopic measurements were conducted before and after the Raman measurements. Previously, CD measurements and thermal melts showed that this technique is sensitive to unfolding of the β-hairpin.[10,17] However, the CD spectra (Supporting Information Figure S4) obtained before and after Raman measurements were similar and were characteristic of a β-hairpin. The magnitude of the ellipticity was the same, within experimental error. These results indicate that the structural changes observed in the UVRR difference experiment, which are substantial (see quantitation below), are reversible.

As a control for irreversible covalent modifications of the peptides, which might be mediated by any reactive oxygen species produced in the sample jet, electrospray ionization MS data were acquired before and after a 244 nm Raman measurement on peptide E. The MS data acquired before and after the measurement were indistinguishable and had the expected parent ion m/z of 2297 (Supporting Information Figures S5 and S6). When the high-power illumination time was increased from 120 to 240 s, there was still no change in the MS data. This experiment shows that there is no detectable covalent modification or cleavage of the peptide during the acquisition of the Raman data.

Interestingly, shifts of the radical CO stretching vibration were observed in peptide C at pD 8.5 (Figure 7D), while peptide A (Figure 7C), peptide E (Figure 7E), and peptide H (Figure 7F) had CO frequencies similar to those of tyrosine (Figure 7A) and the Tyr-His dipeptide (Figure 7B). At pD 8.5, peptide C, which lacks the π–π stacking histidine but has a cross-strand cyclohexylanine, exhibited a 4 cm^{-1} downshifted band, compared to peptide A. This is attributed to a different average conformation of the radical in peptide C, as discussed previously.[11]

DISCUSSION

Peptide maquettes provide an important approach in modeling complex biological reactions in structurally tractable systems.[45–52] This is particularly necessary in the study of ET reactions, which can involve the generation of reactive radicals as intermediates. High-resolution structural determinations can be difficult under these circumstances. In the past, peptide models of redox-active tyrosines have explored their function in α-helical maquettes.[14,16,53] The role of redox-active tryptophan in peptides and small proteins has also been investigated.[15,54–57] Recent work has shown that constraints on

dx.doi.org/10.1021/jp303607b | J. Phys. Chem. B XXXX, XXX, XXX–XXX

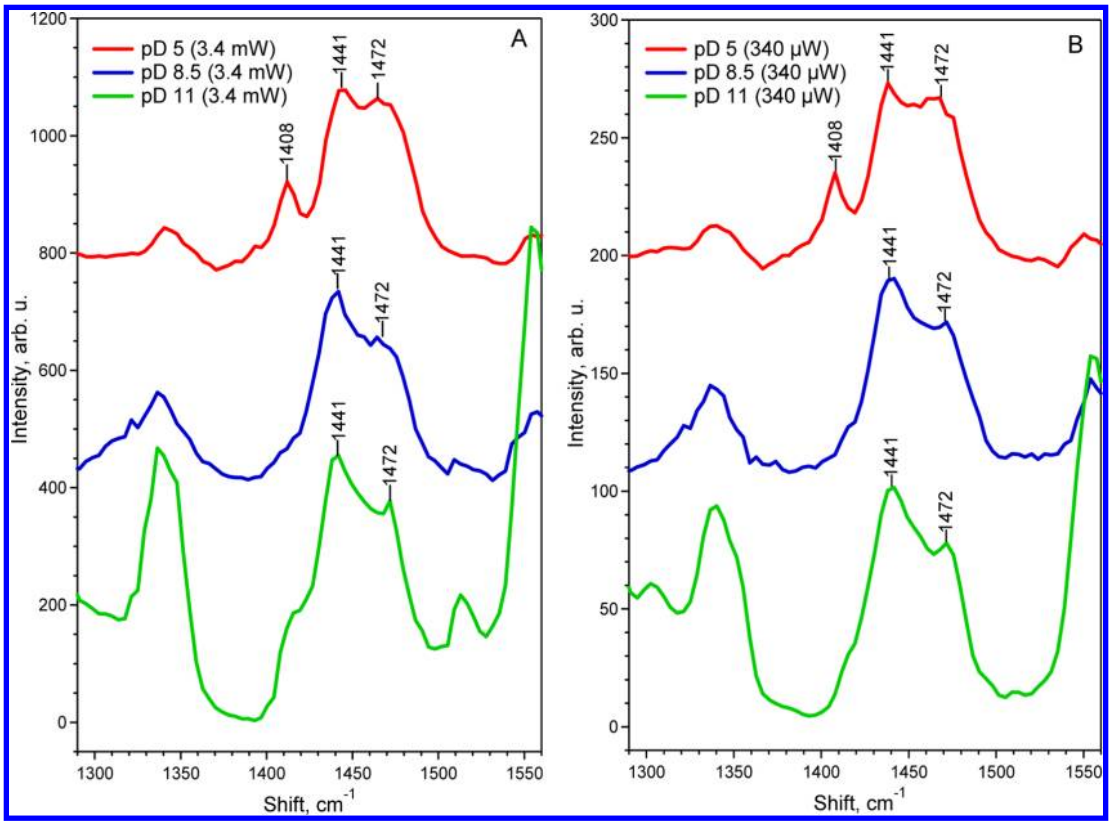

Figure 6. Amide II′ region of the UVRR spectra acquired from peptide E (IMDRYRVRNGDRIHIILR), at three different pD values, showing the 1441 and 1471 cm^{-1} bands. The spectra are repeated from Figure 5. The 244 nm probe power was 3.4 mW (A, left) and 340 μW (B, right). The pD 11 spectrum is in green, the pD 8.5 spectrum is in blue, and the pD 5.0 spectrum is in red.

peptide flexibility can lead to reversible electrochemical behavior for the redox-active amino acid.[14]

However, the effect of redox reactions on biomolecular structure has not yet been systematically explored. The β-hairpin models employed in this study are conformationally flexible and allow us to describe the structural dynamics associated with tyrosine- and tyrosinate-based ET reactions. Here, we use light-induced tyrosine oxidation reactions to show that ET and PCET reactions alter the conformational landscape of the peptide maquettes.

Previous studies described some of the electrochemical and spectral properties of these β-hairpins. CD and thermal melt measurements showed that the β-hairpin scaffold is robust to side-chain substitutions and is thermally stable at both low and high pH. The NMR structure of peptide A was determined, confirming the formation of a stable β-hairpin fold at pH 5.0.[10] EPR signals from the neutral tyrosyl radical were observed after UV photolysis. The signal amplitude decreased at low pH, consistent with the expected increase in potential for protonated tyrosine (see Figure 1B, black, for example), when compared to tyrosinate.[58] Electrochemical experiments investigated the dependence of peak potentials on pH values. Cyclohexylalanine or valine substitutions at histidine 14 eliminated inflection points in a plot of peak potential versus pH. This was interpreted as an elimination of a mid-pH-range PCET reaction between the tyrosine and imidazole ring. Modifications at the hydrogen-bonding arginine 16 or the π–cation interacting arginine 12 increased the peak potential in a pH-independent fashion.[10,17] Although the electrochemical titrations of tyrosine were irreversible, evaluation of the appropriate correction factors, according to previous descriptions,[58] indicated that the correction factors were small.

In this work, the UVRR spectra of the β-hairpins were compared with those of tyrosine, tyrosinate, and dipeptides. With the 244 nm probe wavelength, the UVRR spectra of all of the dipeptides and β-hairpins exhibited amide II′ bands in D_2O buffer. The amide II′ bands were observed in the peptides at pD 5.0, 8.5, and pD 11. The assignment to amide II′ was supported by the magnitude of the solvent isotope shift (100 cm^{-1}). The frequency of the amide II′ (1440–1480 cm^{-1}) bands could be readily distinguished from the ND bend of the deuterated histidine side chain at 1408 cm^{-1}, which was observed at pD 5.0.

The amide II enhancement mechanism at 244 nm has been discussed previously. Amide II and II′ bands were observed with 240 and 245 nm excitation of acetamide, methylacetamide, cyclo(gly-pro)dipeptide, poly(L-glutamic acid), and poly(L-lysine).[32,35,36] It was concluded that resonance with the weak peptide n–π^* transition is not responsible for the amide II′ enhancement.[32,35–37] Two remaining possibilities are resonance with the La transition of the tyrosine side chain or preresonance enhancement of the peptide π–π^* transition (~190 nm). The observation of an amide II′ band in Arg-Glu in Figure 5 argues against the La transition of tyrosine as the primary enhancement mechanism. In agreement, the spectrum of peptide A (Supporting Information Figure 3S), obtained using 229 nm excitation, exhibited a more intense amide II′ band (relative to Y8a) when compared to the spectrum, obtained with a 244 nm probe. This result is consistent with a preresonant π–π^* transition enhancement mechanism because the 229 nm probe wavelength is closer to resonance with the

dx.doi.org/10.1021/jp303607b | J. Phys. Chem. B XXXX, XXX, XXX–XXX

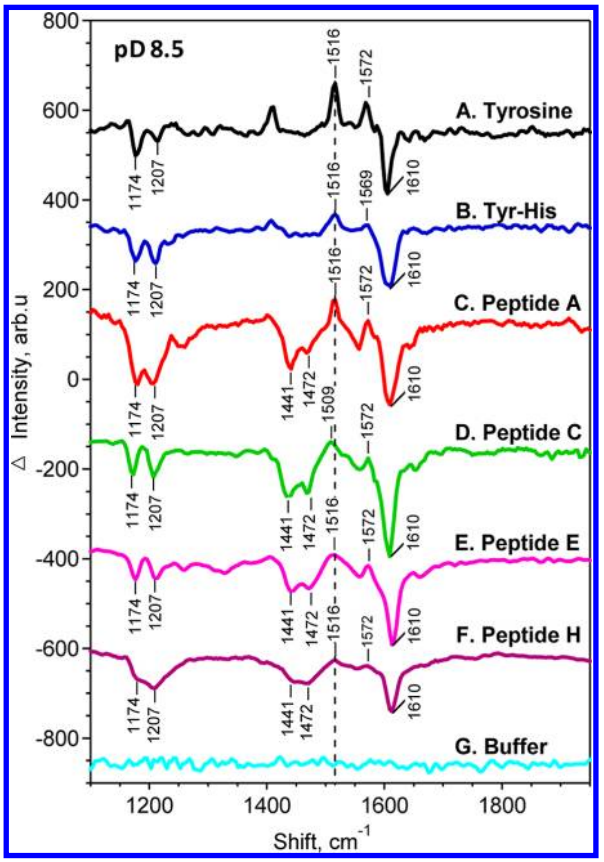

Figure 7. UVRR difference spectra acquired from (A) a tyrosine solution, (B) a Tyr-His dipeptide, (C) peptide A, (D) peptide C, (E) peptide E, and (F) peptide H at pD 8.5. The difference spectra were constructed. Oxidized-minus-reduced (high UV power-minus-low UV power). (G) Negative control, high UV power-minus-low UV power, derived from the buffer alone. A 244 nm probe beam was employed. The vertical dotted line marks the CO band of the neutral tyrosyl radical (A).

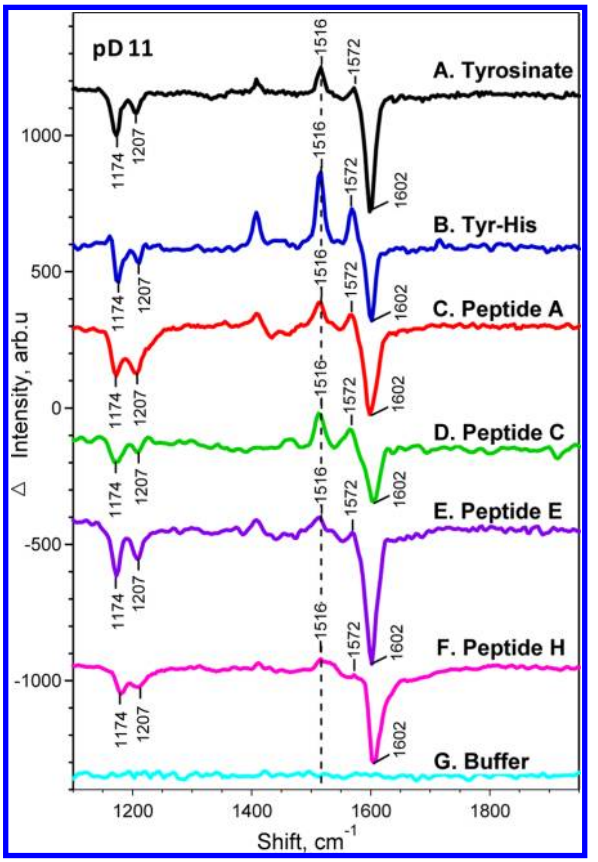

Figure 8. UVRR difference spectra acquired from (A) a tyrosinate solution, (B) a Tyr-His dipeptide, (C) peptide A, (D) peptide C, (E) peptide E, and (F) peptide H at pD 11. The difference spectra were constructed. Oxidized-minus-reduced (high UV power-minus-low UV power). (G) Negative control, high UV power-minus-low UV power, derived from the buffer alone. A 244 nm probe beam was employed. The vertical dotted line marks the CO band of the neutral tyrosyl radical (A).

backbone amide electronic transition. This idea has been suggested previously.[32,35−37]

Two overlapping amide II′ bands were observed in the UVRR spectrum of the β-hairpins, one at 1441 cm^{-1} and the other at 1472 cm^{-1}. The 1472 cm^{-1} frequency is similar to the amide II′ frequencies observed in the dipeptides in D_2O. The downshifted frequency of the 1441 cm^{-1} band is of interest. A ∼1440 cm^{-1} band was observed in the FTIR spectrum of the beta-hairpin-forming peptides, MrH3a and BH8.[59] A ∼1440 cm^{-1} band was also present in the deep UVRR spectrum of β-sheet-forming amyloid fibrils, derived from lysozyme in D_2O.[60] Experimentally, it was observed that the amide II band of dipeptides is sensitive to H bonding, with a 1445 cm^{-1} band identified in non-hydrogen-bonded X-pro dipeptides.[36,39]

DFT calculations on three conformers of gramicidin S, a model for the antiparallel β-sheet, have predicted the infrared spectrum in the gas phase. The conformers differed in the strength of hydrogen-bonding interactions. These calculations were consistent with sequence dependence in the amide II frequency due to side-chain and NH_3^+ coupling. Conformers A, B, and C were predicted to exhibit spectral differences in the amide II region; these spectral changes were attributed to alterations in intramolecular hydrogen bonding.[61] The effect of torsion or twist, which are expected in β-hairpins and β-sheets, was also assessed.[62] A weak dependence of the amide II frequency on the twist angle was reported. Thus, on the basis of the literature, we expect that the frequencies of the amide II′ bands can reflect changes in sequence, interstrand hydrogen bonding, and hairpin torsion. In the future, we will use amide-bond-specific isotopic labeling to distinguish these possible explanations for the downshifted frequency of the 1441 cm^{-1} band.

UVRR difference spectra were acquired from the tyrosine-containing β-hairpins. These data exhibited the characteristic and expected vibrational bands of the tyrosyl radical and of singlet tyrosine or singlet tyrosinate, depending on the pD of the buffer. Interestingly, amide II′ bands also appeared in some of these UVRR difference spectra, showing that changes in intensity of these bands can be coupled with the redox reaction. In the difference spectra acquired at pD 8.5 and 11 from peptide A, two overlapping, negative amide II′ bands were observed with frequencies of 1441 and 1472 cm^{-1}. These results are indicative of an intensity decrease in the CN stretching bands, when tyrosine or tyrosinate oxidation occurs, due to a conformational change (see below). CD spectra (Supporting Information Figure 4S) were recorded before and after the Raman measurements. The CD data were similar, demonstrating that this redox-induced structural change was reversible. This is supported by the indistinguishable mass spectra obtained before and after Raman measurements, which

dx.doi.org/10.1021/jp303607b | J. Phys. Chem. B XXXX, XXX, XXX−XXX

rules out the possibility of covalent modifications of the peptide in the UV probe beam (Supporting Information Figure 5S and 6S). Also, amide II′ bands were observed in peptides C, E, and H at pD 8.5, but not at pD 11, providing additional evidence that UV-induced photodamage was not the origin of these bands.

To determine the magnitude of the conformational change, the amide II′ bands in the high- and low-power spectra were integrated and compared. Oxidation at pD 11 caused a hydrogen-bonding change in ∼20% of the peptide bonds in peptide A but no detectable change in the other peptides (≤10%). Oxidation at pD 8.5 caused a 20−30% percent change in amide hydrogen bonding in all of the peptides. This analysis suggests that approximately five amide bonds were conformationally active at pD 8.5 in all of the maquettes.

A redox-linked conformational change of the β-hairpin explains the negative intensity of the amide II′ bands in the redox-induced difference spectra. This structural alteration can be rationalized as an opening of the β-hairpin due to a decrease in interstrand hydrogen bonding. It has been shown[63] that a β-sheet exhibits a red-shifted $\pi-\pi^*$ absorption compared to an α-helix or a random coil. Excitation at ∼240 nm results in an increased preresonance enhancement of the β-sheet amide band relative to other forms.[34] Therefore, a conformational change that decreases β-sheet interaction energies is expected to decrease amide II′ intensity due to a change in the Raman cross section at 244 nm.

The intensity of the negative amide II′ bands was sensitive to pD in all of the difference spectra obtained from the peptide samples. The origin of this pH dependence is of interest. The only groups expected to titrate in this pH range are the amino terminus (singlet and radical state), tyrosine (singlet state), and histidine due to its pKa upshift (from ∼6 to 9) in the radical state.[10,18]

At pD 8.5, tyrosine transfers a proton when it is oxidized because the pKa of a tyrosine cation radical is below 0 (Figure 1).[7] Histidine becomes protonated in the radical state at this pD.[10] However, this histidine protonation reaction does not underlie the observation of the amide II′ bands. At pD 11, tyrosinate is already deprotonated (Figure 1) in peptide A, and yet, amide II′ bands are observed in the difference spectrum. In addition, amide II′ bands are observed in the difference spectrum of peptide C at pD 8.5, which lacks the histidine.

A more likely explanation for the pD dependence is the protonation of the amino terminus, which is expected at pD 8.5. The amino terminus is then positively charged, generating an electrostatic attraction between the amino and carboxy termini, which is not present at pD 11. The average structure of the peptide A is similar at low and high pD, as judged by the CD.[10] However, the β-hairpin is dynamic and samples an envelope of conformational states, which differ slightly in the strength of interstrand hydrogen-bonding interactions (Figure 2E). The protonated amino terminus, which is formed at pD 8.5, may provide an additional constraint on β-hairpin dynamics, allowing the UVRR difference technique to sample an average change in amide hydrogen bonding. The idea that the hairpins are more dynamic at pD 11, when compared to those at low pD, is supported by the sequence dependence of the amide II′ intensities, which were not detectable in peptides C, E, and H at pD 11. These peptides are expected to be more dynamic because they lack the $\pi-\pi$ interaction between tyrosine and histidine (peptide C) or the hydrogen bond between arginine 16 and tyrosine (peptides E and H). Both of these interactions, which are present in peptide A at this pD, will stabilize the folded structure[17] and may serve to narrow the envelope of hydrogen bond interactions, sampled by the β-hairpin.

Note that the frequencies and intensities in the 1400 cm^{-1} region were similar when the peptide C difference spectrum was compared to the peptide E and peptide H difference spectra at pD 8.5. Peptide C contains a cyclohexylalanine instead of the cross-strand histidine. Thus, the histidine protonation itself is not reflected in the difference spectra at pD 8.5. The expected 1408 cm^{-1} intensity change due to histidine protonation may be too small for detection under these conditions.

Trifluoroacetic acid, which is used as a cosolvent during peptide purification, also has a potential spectral contribution at 1441 cm^{-1}. However, it is expected that this compound will be removed during purification of the peptides. Also, spectral changes in the amide II′ region are dependent on pH. This argues against an assignment of the 1441 cm^{-1} feature to a trifluoroacetic acid contaminant, which would be present at both pD values, when experiments are conducted on the same peptide sample.

These experiments support the conclusion that a PCET or ET reaction can cause a conformational change in tyrosine-containing β-hairpins (as discussed in ref 11). We interpret this conformational change as a decrease in interstrand amide hydrogen bonding in the β-hairpin. This change is reversible, as assessed by control CD and MS experiments. The idea that ET or PCET reactions can substantially alter the secondary structure of the biomolecule may have applicability to more complex reactions. In enzymes, time-dependent fluctuations in solvation, hydrogen bonding, and conformation are important in control of the reaction coordinate, facilitating reactions on different time scales and preventing harmful side reactions. For example, in photosynthetic reaction centers, it has been proposed that dielectric solvation changes, induced by protein dynamics, are important in control of ET.[64,65] In photosystem I, evidence was presented for multiple hydrogen bonding conformers of the primary chlorophyll donor; this was attributed to ET-induced relaxation events.[66] In PSII, solvent and protein dynamics may facilitate the water oxidizing cycle state cycle.[67] Such redox-coupled structural changes were modeled in α-helical, heme-containing maquettes.[68,69]

Here, we show that ET and PCET can induce new minima on the protein conformational landscape in a folded β-hairpin peptide. Such changes in structural coupling may be exploited in biological systems to pump protons, to tune acidity/basicity, and to alter the midpoint potential. Therefore, tyrosine-redox-based structural coupling may play an important role in control of biological reactions.

■ ASSOCIATED CONTENT

Ⓢ Supporting Information

High- and low-power UVRR spectra of tyrosinate, comparison of tyrosinate UVRR difference spectra at pH and pD 11, comparison of UVRR spectra acquired with 229 and 244 nm probes, and comparison of circular dichroism and mass spectra before and after the UVRR measurements. This material is available free of charge via the Internet at http://pubs.acs.org.

dx.doi.org/10.1021/jp303607b | J. Phys. Chem. B XXXX, XXX, XXX−XXX

AUTHOR INFORMATION

Corresponding Author

*E-mail: Bridgette.barry@chemistry.gatech.edu. Phone: 404-385-6085.

Notes

The authors declare no competing financial interest.

ACKNOWLEDGMENTS

Supported by NSF CHE-1213350 (B.A.B.). We thank Prof. Nicholas Hud for the use of CD spectropolarimeter, and Dr. Robin Sibert for the electrochemical titration and CD measurements on Peptide H.

ABBREVIATIONS

Arb. u, arbitrary units; Cha, cyclohexylalanine; MS, mass spectrometry; PCET, proton-coupled electron transfer; PSII, Photosystem II; UVRR, Ultraviolet resonance Raman

REFERENCES

(1) Barry, B. A.; Babcock, G. T. *Proc. Natl. Acad. Sci. U.S.A.* **1987**, *84*, 7099−7103.
(2) Boerner, R. J.; Barry, B. A. *J. Biol. Chem.* **1993**, *268*, 17151−17154.
(3) Barry, B. A. *J. Photochem. Photobiol., B* **2011**, *104*, 60−71.
(4) Stubbe, J.; van der Donk, W. A. *Chem. Rev.* **1998**, *98*, 705−762.
(5) Kulmacz, R. J.; Ren, Y.; Tsai, A. L.; Palmer, G. *Biochemistry* **1990**, *29*, 8760−8771.
(6) Lassmann, G.; Odenwaller, R.; Curtis, J. F.; DeGray, J. A.; Mason, R. P.; Marnett, L. J.; Eling, T. E. *J. Biol. Chem.* **1991**, *266*, 20045−20055.
(7) Dixon, W. T.; Murphy, D. *J. Chem. Soc., Faraday Trans.* **1976**, *72*, 1221−1230.
(8) Harriman, A. *J. Phys. Chem.* **1987**, *91*, 6102−6104.
(9) MacDonald, G. M.; Steenhuis, J. J.; Barry, B. A. *J. Biol. Chem.* **1995**, *270*, 8420−8428.
(10) Sibert, R.; Josowicz, M.; Porcelli, F.; Veglia, G.; Range, K.; Barry, B. A. *J. Am. Chem. Soc.* **2007**, *129*, 4393−4400.
(11) Barry, B. A.; Chen, J.; Keough, J.; Jenson, D.; Offenbacher, A.; Pagba, C. *J. Phys. Chem. Lett.* **2012**, *3*, 543−554.
(12) Högbom, M.; Galander, M.; Andersson, M.; Kolberg, M.; Hofbauer, W.; Lassmann, G.; Nordlund, P.; Lendzian, F. *Proc. Natl. Acad. Sci. U.S.A.* **2003**, *100*, 3209−3214.
(13) Offenbacher, A. R.; Vassiliev, I. R.; Seyedsayamdost, M. R.; Stubbe, J.; Barry, B. A. *J. Am. Chem. Soc.* **2009**, *131*, 7496−7497.
(14) Martinez-Rivera, M. C.; Berry, B. W.; Valentine, K. G.; Westerlund, K.; Hay, S.; Tommos, C. *J. Am. Chem. Soc.* **2011**, *133*, 17786−17795.
(15) Schlamadinger, D. E.; Gable, J. E.; Kim, J. E. *J. Phys. Chem. B* **2009**, *113*, 14769−14778.
(16) Tommos, C.; Skalicky, J. J.; Pilloud, D. L.; Wand, A. J.; Dutton, P. L. *Biochemistry* **1999**, *38*, 9495−9507.
(17) Hughes, R. M.; Waters, M. L. *Curr. Opin. Struct. Biol.* **2006**, *16*, 514−524.
(18) Sibert, R. S.; Josowicz, M.; Barry, B. A. *ACS Chem. Biol.* **2010**, *5*, 1157−1168.
(19) Oladepo, S. A.; Xiong, K.; Hong, Z.; Asher, S. A.; Handen, J.; Lednev, I. K. *Chem. Rev.* **2012**, *112*, 2604−2628.
(20) Chen, J.; Barry, B. A. *Photochem. Photobiol.* **2008**, *84*, 815−818.
(21) Chen, J.; Bender, S. L.; Keough, J. M.; Barry, B. A. *J. Phys. Chem. B* **2009**, *113*, 11367−11370.
(22) Offenbacher, A. R.; Chen, J.; Barry, B. A. *J. Am. Chem. Soc.* **2011**, *133*, 6978−6988.
(23) Jenson, D. L.; Evans, A.; Barry, B. A. *J. Phys. Chem. B* **2007**, *111*, 12599−12604.
(24) Kim, S.; Sacksteder, C. A.; Bixby, K. A.; Barry, B. A. *Biochemistry* **2001**, *40*, 15384−15395.
(25) Schowen, K. B.; Schowen, R. L. *Methods Enzymol.* **1982**, *87*, 551−606.
(26) Johnson, C. R.; Ludwig, M.; Asher, S. A. *J. Am. Chem. Soc.* **1986**, *108*, 905−912.
(27) Asher, S. A.; Ludwig, M.; Johnson, C. R. *J. Am. Chem. Soc.* **1986**, *108*, 3186−3197.
(28) Sharma, B.; Bykov, S. V.; Asher, S. A. *J. Phys. Chem. B* **2008**, *112*, 11762−11769.
(29) Sharma, B.; Asher, S. A. *J. Phys. Chem. B* **2011**, *115*, 5659−5664.
(30) Sension, R. J.; Hudson, B.; Callis, P. R. *J. Phys. Chem.* **1990**, *94*, 4015−4025.
(31) Chen, X. G.; Schweitzer-Stenner, R.; Asher, S. A.; Mirkin, N. G.; Krimm, S. *J. Phys. Chem.* **1995**, *99*, 3074−3083.
(32) Dudik, J. M.; Johnson, C. R.; Asher, S. A. *J. Phys. Chem.* **1985**, *89*, 3805−3814.
(33) Mayne, L. C.; Ziegler, L. D.; Hudson, B. *J. Phys. Chem.* **1985**, *89*, 3395−3398.
(34) Copeland, R. A.; Spiro, T. G. *Biochemistry* **1987**, *26*, 2134−2139.
(35) Song, S.; Asher, S. A. *J. Am. Chem. Soc.* **1989**, *111*, 4295−4305.
(36) Takeuchi, H.; Harada, I. *J. Raman Spectrosc.* **1990**, *21*, 509−515.
(37) Pajcini, V.; Chen, X. G.; Bormett, R. W.; Geib, S. J.; Li, P.; Asher, S. A.; Lidiak, E. G. *J. Am. Chem. Soc.* **1996**, *118*, 9716−9726.
(38) Nielsen, E. B.; Schellman, J. A. *J. Phys. Chem.* **1967**, *71*, 2297−2304.
(39) Jordan, T.; Mukerji, I.; Wang, Y.; Spiro, T. G. *J. Mol. Struct.* **1996**, *379*, 51−64.
(40) Fodor, S. P. A.; Copeland, R. A.; Grygon, C. A.; Spiro, T. G. *J. Am. Chem. Soc.* **1989**, *111*, 5509−5518.
(41) Copeland, R. A.; Spiro, T. G. *Biochemistry* **1985**, *24*, 4960−4968.
(42) Hildebrandt, P. G.; Copeland, R. A.; Spiro, T. G.; Otlewski, J.; Laskowski, M.; Prendergast, F. G. *Biochemistry* **1988**, *27*, 5426−5433.
(43) Caswell, D. S.; Spiro, T. G. *J. Am. Chem. Soc.* **1986**, *108*, 6470−6477.
(44) Range, K.; Ayala, I.; York, D.; Barry, B. A. *J. Phys. Chem. B* **2006**, *110*, 10970−10981.
(45) Gibney, B. R.; Rabanal, F.; Skalicky, J. J.; Wand, A. J.; Dutton, P. L. *J. Am. Chem. Soc.* **1997**, *119*, 2323−2324.
(46) Reedy, C. J.; Gibney, B. R. *Chem. Rev.* **2004**, *104*, 617−650.
(47) Koder, R. L.; Dutton, P. L. *J. Chem. Soc., Dalton Trans.* **2006**, 3045−3051.
(48) Jones, G.; Vullev, V.; Braswell, E. H.; Zhu, D. *J. Am. Chem. Soc.* **1999**, *122*, 388−389.
(49) Cochran, F. V.; Wu, S. P.; Wang, W.; Nanda, V.; Saven, J. G.; Therien, M. J.; DeGrado, W. F. *J. Am. Chem. Soc.* **2005**, *127*, 1346−1347.
(50) Korendovych, I. V.; Senes, A.; Kim, Y. H.; Lear, J. D.; Fry, H. C.; Therien, M. J.; Blasie, J. K.; Walker, F. A.; DeGrado, W. F. *J. Am. Chem. Soc.* **2010**, *132*, 15516−15518.
(51) Chen, X.; Discher, B. M.; Pilloud, D. L.; Gibney, B. R.; Moser, C. C.; Dutton, P. L. *J. Phys. Chem. B* **2001**, *106*, 617−624.
(52) Antonkine, M. L.; Koay, M. S.; Epel, B.; Breitenstein, C.; Gopta, O.; Gärtner, W.; Bill, E.; Lubitz, W. *Biochim. Biophys. Acta* **2009**, *1787*, 995−1008.
(53) Discher, B. M.; Koder, R. L.; Moser, C. C.; Dutton, P. L. *Curr. Opin. Chem. Biol.* **2003**, *7*, 741−748.
(54) Dempsey, J. L.; Winkler, J. R.; Gray, H. B. *Chem. Rev.* **2010**, *110*, 7024−7039.
(55) Shih, C.; Museth, A. K.; Abrahamsson, M.; Blanco-Rodriguez, A. M.; Di Bilio, A. J.; Sudhamsu, J.; Crane, B. R.; Ronayne, K. L.; Towrie, M.; Vlček, A.; Richards, J. H.; Winkler, J. R.; Gray, H. B. *Science* **2008**, *320*, 1760−1762.
(56) Shafaat, H. S.; Leigh, B. S.; Tauber, M. J.; Kim, J. E. *J. Phys. Chem. B* **2008**, *113*, 382−388.
(57) Shafaat, H. S.; Leigh, B. S.; Tauber, M. J.; Kim, J. E. *J. Am. Chem. Soc.* **2010**, *132*, 9030−9039.
(58) Jovanovic, S. V.; Harriman, A.; Simic, M. G. *J. Phys. Chem.* **1986**, *90*, 1935−1939.

(59) Dyer, R. B.; Maness, S. J.; Peterson, E. S.; Franzen, S.; Fesinmeyer, R. M.; Andersen, N. H. *Biochemistry* **2004**, *43*, 11560−11566.
(60) Xu, M.; Shashilov, V.; Lednev, I. K. *J. Am. Chem. Soc.* **2007**, *129*, 11002−11003.
(61) Joshi, K.; Semrouni, D.; Ohanessian, G.; Clavaguera, C. *J. Phys. Chem. B* **2012**, *116*, 483−490.
(62) Bour, P.; Keiderling, T. A. *J. Mol. Struct.* **2004**, *675*, 95−105.
(63) Rosenheck, K.; Doty, P. *Proc. Natl. Acad. Sci. U.S.A.* **1961**, *47*, 1775−1785.
(64) Wang, H.; Lin, S.; Allen, J. P.; Williams, J. C.; Blankert, S.; Laser, C.; Woodbury, N. W. *Science* **2007**, *316*, 747−750.
(65) Wang, H.; Hao, Y.; Jiang, Y.; Lin, S.; Woodbury, N. W. *J. Phys. Chem. B* **2012**, *116*, 711−717.
(66) Bender, S. L.; Barry, B. A. *Biophys. J.* **2008**, *95*, 3927−3934.
(67) Polander, B. C.; Barry, B. A. *Proc. Natl. Acad. Sci. U.S.A.* **2012**, *109*, 6112−6117.
(68) Shifman, J. M.; Moser, C. C.; Kalsbeck, W. A.; Bocian, D. F.; Dutton, P. L. *Biochemistry* **1998**, *37*, 16815−16827.
(69) Grosset, A. M.; Gibney, B. R.; Rabanal, F.; Moser, C. C.; Dutton, P. L. *Biochemistry* **2001**, *40*, 5474−5487.